Carbohydrate Research 555 (2025) 109586

Contents lists available at ScienceDirect

Carbohydrate Research

journal homepage: www.elsevier.com/locate/carres

Unveiling the structure of *Delftia acidovorans* Lipopolysaccharide: insights into O-antigen and lipid A

Anna Notaro [a], Luisa Sturiale [b], Angelo Palmigiano [b], Domenico Garozzo [b], Immacolata Speciale [a,*]

[a] Department of Chemical Sciences, University of Napoli Federico II, I-80126 Napoli, Italy
[b] CNR, Institute for Polymers, Composites and Biomaterials, 95126 Catania, Italy

ARTICLE INFO

Keywords:
Gram-negative bacterium
O-Antigen polysaccharide
Lipid A
Structural determination
NMR
MALDI

ABSTRACT

Delftia acidovorans is a Gram-negative bacterium traditionally considered as an environmental organism, although it has recently been identified as an opportunistic pathogen in immunocompromised patients. Furthermore, this bacterium was also recognized as part of the crypt-specific core microbiota in healthy mice. Despite its detection in various contexts, the chemical structure of its lipopolysaccharide (LPS) remains uncharacterized.

Here, the structure of O-antigen and lipid A from *Delftia acidovorans* were characterized by combining chemical approaches with spectroscopic and spectrometric studies. In detail, the O-antigen is found to consist of a novel glycan sequence composed of 3)-α-L-rhamnose-(1→4)-α-D-glucose-(1→ disaccharide in the linear backbone, where glucose is in turn branched at the O-2 position with a β-D-*N*-acetyl-glucosamine, that is non-stoichiometrically acetylated at position O-6. Whereas lipid A is predominantly represented by a hexa-acylated species with a symmetric distribution of acyl chains.

1. Introduction

Delftia acidovorans is a Gram-negative bacterium belonging to the Betaproteobacteria class (order Burkholderiales) formerly classified as *Comomonas acidovorans*, until a detailed phylogenetic study revealed its placement in the newly established genus *Delftia* [1]. It is an aerobic, saprophytic, non-fermentative [2–4], slightly curved rod-shaped bacterium that can exist as a single cell or in pairs. Its size ranges from 0.4 to 0.8 μm in width and 2.5–4.1 μm in length [1,2] and it has one to five flagella that give it motility [1]. *D. acidovorans* is an environmental mesophilic bacterium found in water and soil with minimal or no salt concentrations. Interestingly, this bacterium i) is able to metabolize gold, together with *Cupriavidus metallidurans* [5,6]; ii) converts toxic metals, including selenium and chromium ions, into harmless ones, making it valuable for bioremediation processes [7]; and iii) produces polyhydroxyalkanoates (PHAs) that can serve as a sustainable alternative to traditional plastics in manufacturing sector [8].

Although *D. acidovorans* was long viewed as an environmental bacterium lacking clinical relevance for humans, it has recently been described as an opportunistic pathogen in both immunocompetent [4,9] and immunocompromised patients [4,10,11]. It has been recognized as a cause of clinical conditions, such as pneumonia, urinary tract infections, endocarditis, peritonitis, catheter-related infections and bacteremia [12], as well as a causative agent of nosocomial infections [13,14].

Recent studies have also demonstrated that the lipopolysaccharide (LPS) molecule from the *D. acidovorans* bacterium is a major component of the crypt-specific core microbiota (CSCM) in cecal and proximal colonic crypts of healthy mice [15], playing a crucial role in epithelial regeneration, control of intestinal epithelium proliferation and cell differentiation [16]. Therefore, understanding the chemical structure of the LPS molecule produced by *Delftia acidovorans* is a key point to study the relationship between structure and function. This is an important aspect if we consider that it has recently been demonstrated that the long-term view of LPS as a toxic molecule has been subverted and that behind this difference in toxicity there is a difference in chemical structure [17].

LPS is a macromolecule composed of three domains: a conserved phosphoglycolipid (lipid A, usually consists of two D-glucosamine linked via a β(1→6) glycosidic bond, generally bearing a phosphoryl group at

* Corresponding author.
E-mail address: immacolata.speciale@unina.it (I. Speciale).

https://doi.org/10.1016/j.carres.2025.109586
Received 11 April 2025; Received in revised form 11 June 2025; Accepted 17 June 2025
Available online 18 June 2025

positions 1 and 4′, to which the acyl chains are attached), the oligosaccharide chain (named core OS region) and a O-polysaccharide (also termed O-antigen or O-specific chain) that is exposed to the external environment, which may be missing creating a differentiation of these molecules into rough (R-type) and smooth (S-type) types [17]. The latter exhibits great variability even among bacteria of the same species, and its structure can be modulated in response to environmental factors.

Hence, in this study, both the lipid A and O-antigen polysaccharide structures of *Delftia acidovorans* from the CSCM of healthy mice were isolated and characterized. From a chemical point of view, LPS presented a new O-antigen structure consisting of a trisaccharide skeleton, whereas the lipid A part is a mixture of tetra-, penta- and hexa-acylated species even if the latter is the most abundant, in agreement with literature data [16].

2. Material and methods

2.1. LPS purification

D. acidovorans was isolated from the proximal colon tissues of healthy mice according to the procedure described by Naito et al. [16]. Thus, the crude material was lyophilized obtaining 13.703 g of dried cells which were extracted by hot phenol/water method [18,19]. Each phase was dialyzed against Milli-Q water using a 12–14 kDa cut-off membrane (Cod. 15320762, Fisher Scientific) and then freeze-dried, obtaining 0.406 g for the aqueous phase and 0.849 g (yield 6.2 %) for the phenolic phase. Both fractions were checked via SDS-PAGE analysis (13,5 % polyacrylamide gel) in denaturing conditions and visualized by silver nitrate staining [18,20], disclosing the presence of LPS in both phases. However, the phenolic phase was used for further analyses as it produced a larger amount of sample. Therefore, it was dissolved in 40

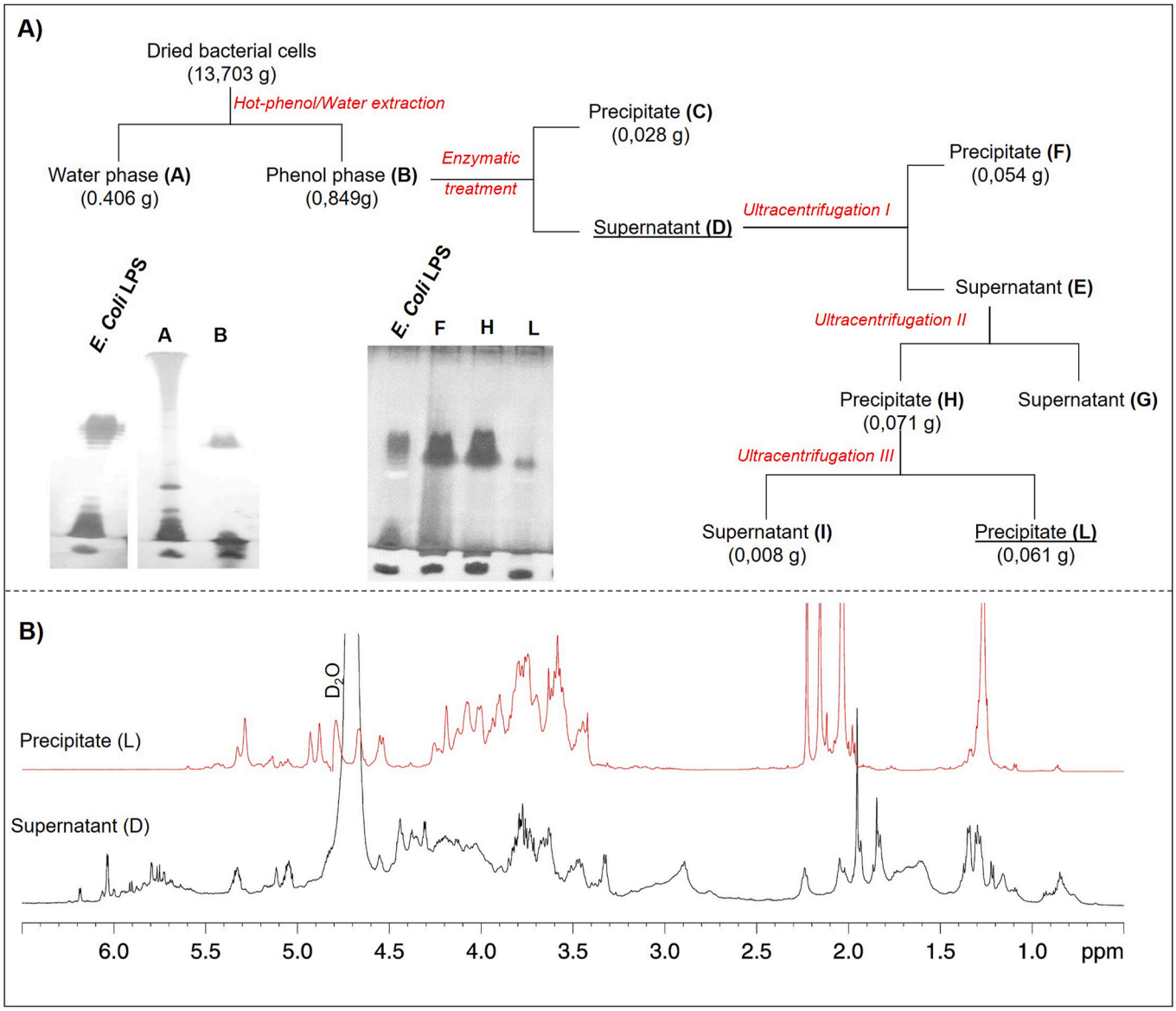

Fig. 1. A) Schematic procedure of LPS purification from *D. acidovorans* bacterial cells. Enzymatic treatment was performed with DNAse, RNAse and Protease as detailed in the paragraph 2.1. Both water and phenol phases (**A** and **B**, respectively) together with the purified sample after the ultracentrifugation steps (**F**, **H** and L) were analyzed via SDS-PAGE (shown in the insert) using a polyacrylamide gel at 12 % and silver staining. *E. coli* LPS was used as standard. The ultracentrifugation conditions are as follows: I. 30000 rpm, 4 °C, 1 h; II. 40000 rpm, 4 °C, 5 h; III. 30000 rpm, 4 °C, 17 h. **B)** (600 MHz, 298 K, D_2O). Comparison of the ^1H NMR spectrum of the phenol phase after the enzymatic treatment (supernatant **D**) and after three steps of ultracentrifugation (precipitate **L**). The precipitate **L** represents a pure LPS sample compared to the supernatant **D** in which the nucleic acid (6.2–5.6 ppm) and protein (1.3–0.7 ppm) signals are detectable.

mL of digestion buffer (100 mM Tris-HCl, 50 mM NaCl, 10 mM $MgCl_2$, pH 7.5), to which 4 mg of DNAse (DN25-Sigma Aldrich) and 4 mg of RNAse (R5503-Sigma Aldrich) were added and incubated at 37 °C under stirring. After 16 h, 2 mg of protease (P5147-Sigma Aldrich) was added and left for another 6 h. Then, the mixture was centrifuged (5000 *g*, at 25 °C for 15 min): the precipitate (0,028 g) was preserved and the supernatant was ultracentrifuged (SW-41 rotor for Beckman centrifuge) according to the scheme shown in Fig. 1. In detail, the supernatant was centrifuged at 30000 rpm, 4 °C for 1 h obtaining a precipitate that was set aside a supernatant that was centrifuged again (40000 rpm, 4 °C, 5h). The precipitate, containing LPS material, was dissolved in water and centrifuged again (30000 rpm, 4 °C, 17h) to obtain pure LPS used for further investigation.

2.2. Isolation of the O-antigen and lipid A portions

To separate the lipid A moiety from the entire LPS, a mild acid hydrolysis was performed suspending 6 mg of LPS in 600 μl of 1 % acetic acid and incubating at 100 °C for 6 h [21], until a white solid appeared at the bottom. Therefore, the lipid A was separated from the supernatant, containing the sugar fraction (O-antigen polysaccharide), by centrifugation (5400 g, 15 min at 25 °C), and they both were freeze-dried, obtaining a final yield of 1 mg for the lipid A and 4 mg for O-antigen polysaccharide.

2.3. Deacetylation of the O-antigen

NMR studies disclosed the presence of acetyl groups; therefore, to have simplest spectra helpful for the correct assignment of the O-antigen polysaccharide structure, the deacetylation of the sample was performed. In detail, an appropriate volume of ammonia solution (with a final concentration of 33 %) was added directly on the O-antigen sample used for the NMR analysis. The mixture was then incubated for 1 h at 37 °C and, then purified on Biogel P10 resin (Column volume: 110.4 mL; flow: 8,4 ml/h) using a 50 mM ammonium bicarbonate solution as eluent. The eluate was monitored by a refractive index detector (Knauer K-2310) and fractions were pooled accordingly and checked via ^{1}H NMR, revealing that the deacetylated O-antigen was eluted at one third of the column volume with a yield of 1 mg.

2.4. Compositional analysis of LPS and lipid A

Monosaccharide content was established by derivatizing the LPS (0.5 mg; precipitate **L** in Fig. 1a) as (i) acetylated methyl glycoside (AMG) to elucidate the sugar components; (ii) partially methylated alditol acetate (PMAA) to establish the sugar substitution pattern; and (iii) acetylated octyl glycosides (AOG) to determine the sugar absolute configuration [18,21,22]. Briefly, the AMG consists of two steps of reaction: methanolysis dissolving the sample in methanol hydrochloride solution ~1.25 M and incubating it at 80 °C for 16 h, followed by acetylation step (with pyridine and Acetic anhydride). The AAPM derivatization, instead, involves four reaction steps: methylation (with methyl iodide in Dimethyl sulfoxide); hydrolysis (with trifluoroacetic acid 2 M, at 120 °C, for 2h); reduction with sodium borodeuteride ($NaBD_4$); acetylation (as before). As OAG, they were obtained incubating the sample in pure octanol and acetyl chloride, at 60 °C, for 16 h, followed by acetylation step. Fatty acids composition analysis was carried out on a pure lipid A, as reported De Castro et al., 2010 [18].

All derivatives were analyzed via Gas Chromatography – Mass Spectrometry technique using a GC instrument Agilent 6850 coupled to MS Agilent 5973, equipped with a SPB-5 capillary column (Supelco, 30 m × 0.25 i.d., flow rate, 0.8 mL min^{-1}) and He as carrier gas. Electron impact mass spectra were recorded with an ionization energy of 70 eV and an ionizing current of 0.2 mA. The temperature program was set as follows: 150 °C for 5 min, 150 → 280 °C at 3 °C/min, 300 °C for 5 min, except for the detection of C8:0 (3-OH) which is a very short fatty acid and needs a different program (80 °C for 4 min, 10 °C/min up to 280 °C).

2.5. NMR spectroscopy

1D and 2D NMR spectra were carried out on a Bruker DRX-600 spectrometer equipped with a cryoprobe, by dissolving the samples in D_2O. Acetone was used as internal standard (^{1}H: 2.225 ppm; ^{13}C: 31.45 ppm) to calibrate spectra. All spectra were acquired at 298 K.

Parameters used for the analysis of the O-antigen before and after the deacetylation, are as follows. For the polysaccharide before the treatment, homonuclear experiments (COSY, TOCSY and NOESY) were recorded using 512 FIDs of 2048 complex data points, acquiring 24 scans and using a mixing time of 200 ms for both TOCSY and NOESY spectra acquisition. Heteronuclear experiments (HSQC and HMBC) were acquired using data sets of 512 × 2048 points with 24 scans per FID. As for the experiments of the O-antigen after the deacetylation treatment, instead, 1024 FIDs of 2048 complex data points were collected for the homonuclear experiments, acquiring 24 scans for FID. A mixing time of 200 ms were used for both TOCSY and NOESY spectra acquisition. Heteronuclear experiments, instead, were acquired using data sets of 1024 × 1024 points with 32 scans per FID for the HSQC and 512 size of FIDs of 2048 data points with 64 scans for the HMBC spectrum. All spectra were processed and analyzed using the standard Bruker Software (TopSpin 3.6).

2.6. MALDI/MS analysis of lipid A

Reflectron MALDI-TOF mass spectra and MALDI TOF/TOF MS/MS of the lipid A molecule was performed [21,23] in negative ion mode, using a 4800 Proteomic Analyzer (Applied Biosystems) supplied with a Nd:YAG laser (at λ 355 nm). Mass accuracy was about 50 ppm. The matrix solution was prepared by dissolving 5-Chloro-2-mercaptobenzothiazole in methanol/0.1 % TFA/acetonitrile (ratio 7:2:1 in vol) at a concentration of 75 mg/mL. A sample/matrix solution mixture (1:1 v/v) was deposited (1 μL) on a MALDI plate and dried at room temperature. The experiment was performed in triplicate and raw data were processed by using DataExplorer™ 4.9 software.

3. Results and discussions

3.1. LPS isolation and GC-MS analysis

Dried cells of *D. acidovorans* were extracted by hot phenol/water method [19] to isolate LPS material [18]. SDS-PAGE analysis of aqueous and phenolic fractions (**A** and **B**, respectively) disclosed the presence of LPS material in both (Fig. 1A). However, the analyses were continued on the phenol phase, which was the one with an adequate amount of crude LPS material. Therefore, it was purified through enzymatic treatment, followed by sequential ultracentrifugation steps as described in Fig. 1A. Further SDS-PAGE analysis revealed the presence of pure LPS material in the third ultracentrifugation precipitate (fraction **L**, Fig. 1A). In agreement, proton NMR analysis (Fig. 1B) no longer showed nucleic acids and protein material (signals ranging from 6.2 to 5.6 ppm and 1.3–0.7 ppm, respectively), in contrast with the spectrum of the sample not subjected to ultracentrifugation (supernatant **D**).

Pure LPS (fraction **L**) was used for chemical composition by derivatizing it as acetylated *O*-methyl glycosides, revealing the presence of rhamnose (Rha), glucose (Glc), glucosamine (GlcN) and 3-deoxy-D-*manno*-2-octulosonic acid (Kdo, a signature of LPS molecules; Fig. S1A). Linkage analysis was also performed as described elsewhere [18] obtaining mainly the following monosaccharides (Fig. S1B): 3-substituted Rha, 2,4-di- substituted-Glc, terminal-GlcN and a peak at 36.94 min that was attributed to an alditol disaccharide, obtained as a result of an incomplete hydrolysis of the polysaccharide. The disaccharide alditol was identified as a glucopyranoside linked at position O-3 of the rhamnose alditol (Fig. S1C). The ions at *m/z* 131 and 118 are

representative of the 3-substituted 6-deoxy hexose, whereas the *m/z* 275 ion suggested that the other residue was glucopyranose, since this is the value of the oxonium ion of the methylated glucopyranose linked at O-3 and O-6. Instead, ions at *m/z* 388 and *m/z* 322 were indicative of the fact that it is a disaccharide. Indeed, *m/z* 388 fragment comes from the loss of two acetic acid molecules from the alternative molecular ion (*m/z* 508, derived from a carbon loss in position 6 of glucopyranose; Fig. S1C); *m/z* 322 fragment, instead, corresponds to the J fragment [24]. Finally, acetylated 2-*O*-octyl glycosides derivatives allowed to establish that the absolute configuration of two sugar residues is D except for the rhamnose which is L.

3.2. Isolation of O-antigen polysaccharide and lipid A

To exactly define the structure of the whole LPS, it was split into two components (O-antigen polysaccharide and lipid A) by mild hydrolysis with 1 % acetic acid [21] and studied separately as detailed in the following paragraphs.

3.2.1. O-antigen polysaccharide structural characterization via NMR spectroscopy

The structure of the O-antigen polysaccharide isolated from *D. acidovorans* was established via NMR spectroscopy. Proton NMR spectrum (Fig. 2A) showed an intense peak at 1.27 ppm typical of a methyl group of a 6-deoxy-monosaccharide, two sharp peaks at 2.15 and 2.03 ppm, diagnostic of the O-linked and the N-linked acetyl groups, respectively, a crowded carbinolic region (4.25–3.44 ppm) and several signals (maybe 6) in the anomeric region (5.4–4.5 ppm). However, analysis of the HSQC spectrum (Fig. S2A) revealed that the peak at δ_H 4.54 ppm correspond to a density which carbon chemical shift value is *65.1* ppm (labelled as **C′**$_6$ in Fig. S2A), i.e., not ascribable to an anomeric signal, but it had the typical chemical shift values of an H-6 proton of an acetylated monosaccharide [25]. However, densities of a C-6 carbon signal of a not acetylated sugar were recognized in the HSQC spectrum (**C**$_{6/6'}$ in Fig. S2A), implying that the acetylation on the six position was not stoichiometric. Therefore, to simplify the spectra, the O-antigen polysaccharide was O-deacetylated by dissolving the sample in 33 % ammonia solution (at 37 °C for 1 h) and then, a purification on size exclusion chromatography Biogel-P10 was performed (data not shown). Proton NMR analysis of all obtained fractions revealed the presence of pure deacetylated O-chain (Fig. 2B) in the first part of the column. Comparing the ^{1}H NMR spectrum with the one before the treatment (Fig. 2A), it was immediately evident that proton signals at 4.54 and 2.15 ppm chemical shift values, attributable to H-6 of an acetylated monosaccharide and the acetyl group respectively, disappeared. Moreover, both anomeric and carbinolic regions appeared less crowded and clearer, indeed, anomeric region showed only three signals instead of six (Fig. 2). All of this proved that the polysaccharide was partially acetylated, as suggested above.

Therefore, the structure of the deacetylated sample was established recording all homo- and heteronuclear 2D NMR spectra (COSY, TOCSY, NOESY, ^{1}H–^{13}C HSQC and ^{1}H–^{13}C HMBC).

Residues are defined with capital letters from **A** to **C** following the decreasing chemical shift values order as reported in Fig. 2. Residue **A** is a 2,4-linked α-glucose. The *gluco* stereochemistry was inferred by the efficient transfer magnetization in the TOCSY spectrum, which showed the correlation from proton H-1 up to H-5 (Fig. 3A). The α-configuration of the anomeric carbon, instead, was established based on the proton and carbon chemical shift values (^{1}H: 5.33 ppm/^{13}C: *97.*0 ppm) and confirmed by a small coupling constant $^3J_{H1,H2}$ that resulted in a sharp single peak in the proton spectrum (Fig. 3A). Moreover, the HSQC spectrum (Fig. S2B) displayed that both C-2 (at *82.*4 ppm) and C-4 (at *78.*1 ppm) carbon densities resonated at lower fields compared to those of the unsubstituted residue (*72.*2 ppm and *70.*6 ppm, respectively) [25], indicating that these positions are glycosylated. These data aligned with NOESY correlations between H-1 of **B** with H-4 of **A**, and H-1 of **C** with H-2 of **A** (Fig. 3B).

Regarding the residue **B**, the anomeric proton showed only one correlation in the TOCSY spectrum, whereas H-2 displayed correlations with all other proton rings (Fig. 3A), a typical pattern of a *manno*-configured sugar [25]. Furthermore, in the COSY experiment, starting from the H-5 proton, it was possible to identify the H-6 as a methyl group which resonated at 1.27 ppm (Table 1), recognizing this residue as a rhamnose unit. In addition, based on the chemical shift value of both C-1 (^{1}H: 4.93 ppm/^{13}C: *101.*4 ppm) and C-5 (*70.*2 ppm) carbon densities (Fig. S2B, Table 1), it was possible to establish that **B** residue has α-configured at the anomeric carbon [25,26]. Moreover, the glycosylation shift at low field of the carbon C-3 (*77.*5 ppm) compared with the unsubstituted residue (*71.*3 ppm) [25] indicated that this residue was 3-substituted. Accordingly, correlations between H-1 of **A** and H-3 of **B** appeared in the NOESY spectrum (Fig. 3B).

By using a similar approach, the residue **C** was recognized as

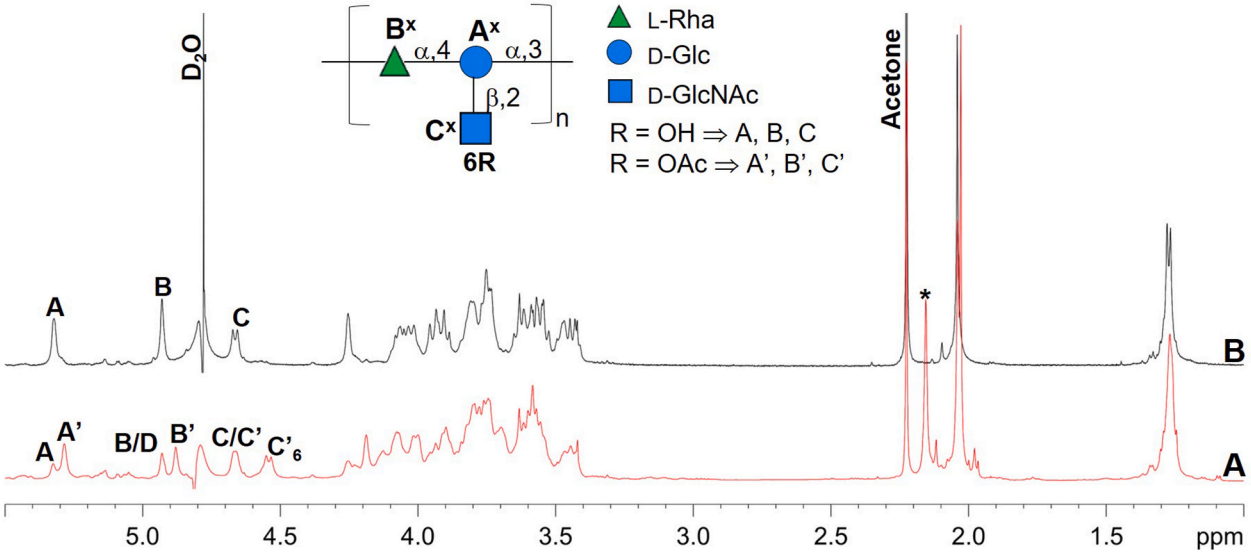

Fig. 2. (600 MHz, 298 K, D_2O). ^{1}H NMR spectra of the O-Chain of *D. acidovorans* before (**A**) and after (**B**) the deacetylation treatment. The letters follow the system of Table 1 and Fig. S2. In detail, **A**, **B**, and **C** refer to the non-acetylated block, while **A′**, **B′** and **C′** to the acetylated one, as indicated in the figure. The structure is represented according to the symbol as defined by the rules of the Symbol Nomenclature of Glycans (SNFG) [24].

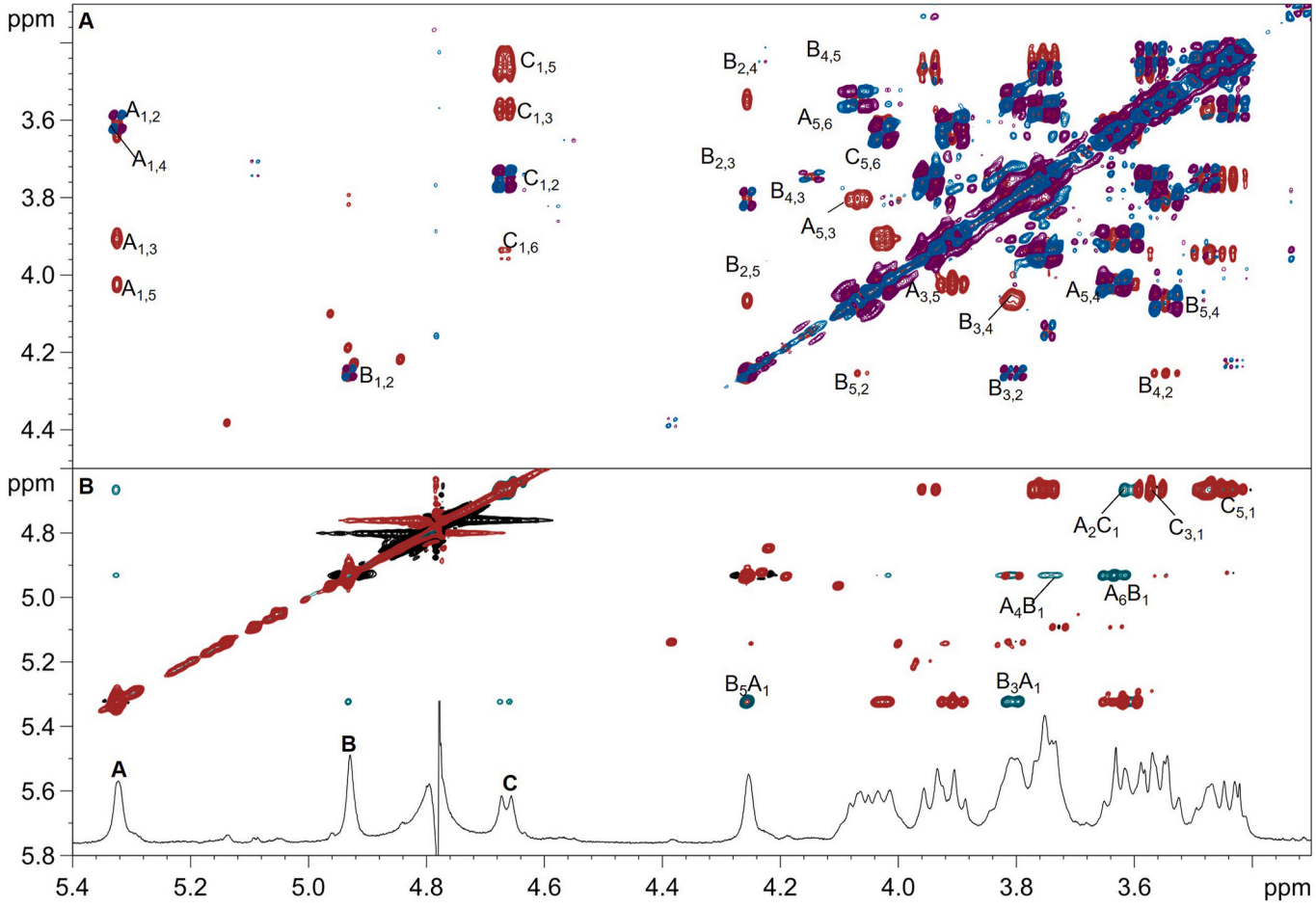

Fig. 3. Homonuclear spectra of the O-Chain of *D. acidovorans* after the deacetylation treatment recorded at 600 MHz, in D_2O, at 298 K. **A**. Overlay of TOCSY (red) and COSY (violet and blue) spectra. **B**. Superimposition of TOCSY (red), NOESY (light blue) and proton spectra. Letters follow the system of Table 1. Important correlation densities were highlighted in the figure.

terminal β-*N*-acetyl-glucosamine linked to O-2 of **A**, as evidenced by the NOE correlations (Fig. 3B). Both COSY and TOCSY spectra confirmed the *gluco* stereochemistry of the residue. Furthermore, the anomeric signal (at 4.66 ppm) in the proton spectrum (Fig. 3B) appeared as duplet with a large coupling constant $^3J_{H1,H2}$ value (8.3 Hz), characteristic of a residue β-configured at the anomeric center; also confirmed by the presence of the $H_{1,3}$ and $H_{1,5}$ diaxial correlations (Fig. 3A).

Therefore, NMR data demonstrated that the structure of the deacetylated O-polysaccharide consists of a trisaccharide repeating unit formed by →3)α-Rha(1 → 4)-α-Glc(1→ as a linear backbone, to which the β-D-*N*-acetyl-glucosamine (**C**) is linked at the position O-2 of the glucose (the structure is schematized in Fig. 2).

Interpretation of these simplified spectra can help with the studies of a more complex spectra recorded for the O-antigen structure (Fig. 4, S2A and S3). Indeed, overlapping the HSQC spectrum of the O-antigen with that of the deacetylated one, it was clear that residues **A**, **B** and **C** are completely overlapped, and thus were recognized as 2,4-Glc, 3-Rha and t-GlcNAc, respectively. However, some densities were out of this allowing to establish the presence of three alternative spin systems: **A′**, **B′** and **C'**. The biggest difference was observed for the **C′** residue: combining all homo- (Fig. 4) and heteronuclear experiments, it was possible to recognize this residue as a t-β-GlcNAc with the acetyl group at position O-6, indeed carbons C-6 resonated at *65.*1 ppm, instead of *62.*0 ppm (Fig. S2B, Table 1) with a consequent shift of the C-5 carbon density at *74.*6 ppm. The presence of this additional acetylated group caused a variation of the chemical environment of the other monosaccharides as well, justifying the occurrence of additional anomeric proton signals (Fig. 2A). In detail, **A′** is recognized as an α-glucose 2,4-linked similarly to the **A** residue, with the difference of the density attributed at carbon C-4 that resonated at *77.*6 ppm (Table 1, Fig. S2). Interestingly, the analysis of the NOESY spectrum (Fig. 4C) showed a correlation between proton H-1 of **C** and H-2 of **A**, and correlation between H-1 of **C′** and H-2 of **A′**, confirming that depending on whether the t-β-GlcNAc is acetylated or not in position 6, there is a variation in residue **A** and, therefore, the acetylation is not stoichiometric. Similarly, both **B** and **B′** are a 3-linked α-rhamnose with a slight difference in the chemical shift value of the C-3 density as consequence of the presence of the **C′** residue. As before, NOESY spectrum (Fig. 4C) was helpful in the differentiation between the two: H-1 of **B** correlates with H-4 of **A** and H-1 of **B'** with H-4 of **A'**. Interestingly, a deeper inspection of the HSQC spectrum (Fig. S2A) revealed the presence of an additional monosaccharide, labelled with letter **D**, recognized as another 3-*O*-substituted-α-rhamnose unit with a methyl group at position O-3, as suggested by the carbon C-3 chemical shift value at *80.*8 ppm. This interpretation was also confirmed by the HMBC correlation between carbon C-3 of the **D** residue and a methyl group at *57.*3 ppm (Fig. S3; Table 1). This residue may indicate the termination of the O-Antigen polymerization, suggesting that when the methyl group occurring at position O-3 functions as cap.

Concluding, the O-chain polysaccharide structure of *Delftia* consists of an alternating acetylated and non-acetylated repeating unit, but the specific repeating pattern remained elusive. However, integrating the C-5 densities of both t-β-GlcNAc with and without the acetyl group at position O-6 (namely **C'** and **C** residues, respectively) resulted that the

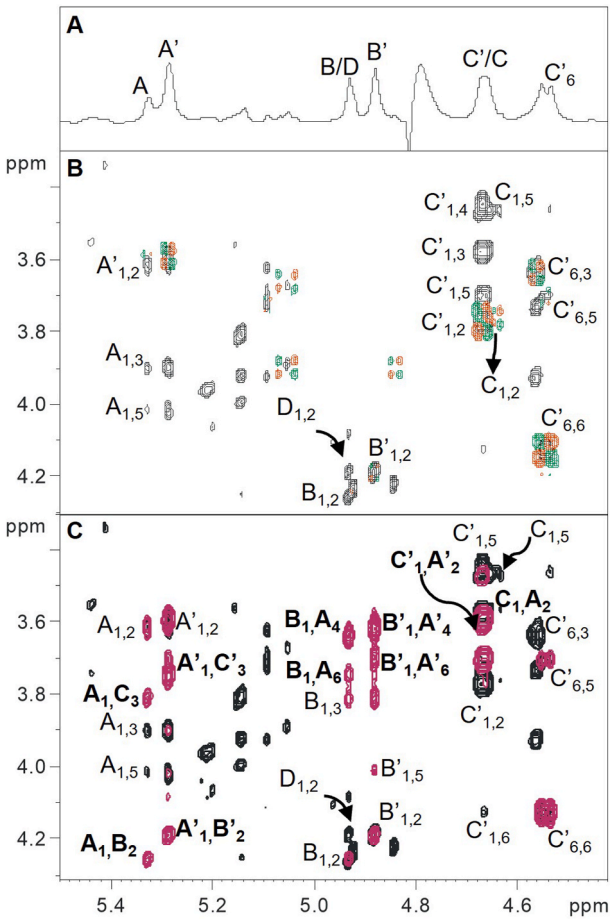

Fig. 4. ^{1}H-^{1}H Homonuclear spectra of the O-Chain of *D. acidovorans*. **A**) proton spectrum; **B**) overlay of the TOCSY (black) and COSY (red and green) spectra; **C**) overlay of the TOCSY (black) and NOESY (dark pink) spectra. The letters used for the annotation of densities follow the system of Table 1.

acetylated ones were dominant (ratio between acetylated: not-acetylated repeating units was 2:1).

3.2.2. *Lipid A structural determination*

An aliquot of pure LPS was subjected to a mild acid hydrolysis obtaining a pure lipid A, which was used to determine the fatty acids composition, revealing the occurrence of short-chain fatty acids: C8:0 3-OH, C10:0 3-OH and C12:0, C14:00, C16:0, C18:0 (data not shown). This finding aligns with the MALDI-MS (Matrix-Assisted Laser Desorption Ionization-Mass Spectrometry) analysis [21], which identified three series of molecular ions corresponding to tetra-, penta- and hexa-acylated species (labelled with **a**, **b** and **c**, respectively), with the hexa-acyl species as the most abundant among the three (Fig. 5, Table S1). The peak at *m/z* 1463.95 (**c$_2$**) was attributed to the *mono*--phosphorylated hexa-acylated lipid A, which differed from ion at *m/z* 1543.9 (**c$_3$**) by a phosphate group, thus identifying the latter as a bis-phosphorylated specie ($\Delta m/z = 80$), whereas the ion at *m/z* 1435.9 (**c$_1$**) differed from **c$_2$** by the replacement of C16:0 with C14:0. Starting from ion **c$_2$**, the composition of the homologous species in each group was identified: **a$_3$** (*m/z* 1111.66) corresponded to a molecular ion lacking a C10:0 (3-OH) and a C12:0 ($\Delta m/z = 352.29$), while **b$_2$** species ($\Delta m/z = 170$) was consistent with the lack of one C10:0 (3-OH). Likewise, the other penta-acylated species differed from **c$_2$** for the absence of one of the two secondary fatty acids, alternatively C12:0 or C16:0 (Fig. 5, Table S1).

The structure of the lipid A of *Delftia* was completely elucidated by negative-ion MALDI MS/MS spectra of peaks at *m/z* 1111.66 (**a$_3$**), 1293.82 (**b$_3$**) and 1463.95 (**c$_3$**), thus defining the exact distribution of the primary and secondary fatty acids between the GlcN I and the GlcN II residues (Fig. 5B–D). The fragment at *m/z* 624.4 (Fig. 5B) originated from the cleavage between C3 and C5 of the GlcN I ($A_2^{3,5}$ Domon and Costello nomenclature [25]), thus indicating that the non-reducing glucosamine (GlcN II) carries a C10:0 (3-OH) and C8:0 (3-OH). The composition of the GlcN II was also confirmed by the peak at *m/z* 672.4, which represents the GlcN II with its fatty acids, after the cleavage between C1 and C3 of the GlcN I ($A_2^{1,3}$). In addition, the peak at *m/z* 923.7 matched with the loss of a C10:0 (3-OH) from the precursor ion (*m/z* 1111.6), thus indicating that this primary fatty acid is ester-linked at the position 3' of the GlcN II. Once defined the substitution pattern of the GlcN II, it was straightforward to establish that the GlcN I carried a C8:0

Table 1
Proton and carbon chemical shift values of the O-Antigen of *D. acidovorans* after and before the deacetylation treatment. **C** residue is N-acetylated (^{1}H:2.04 ppm/^{13}C: *23.*5 ppm), whereas **C**′ is both N- and O-acetylated at position O-6 (^{1}H: 2.15 ppm/^{13}C: *21.*7 ppm). Residue **D** is methylated at position O-3 (^{1}H: 3.41 ppm/^{13}C: *57.*0 ppm).

After deacetylation		**1**	**2**	**3**	**4**	**5**	**6**
A	^{1}H	5.33	3.61	3.91	3.63	4.02	3.75–3.83
2,4-α-Glc	^{13}C	*97.0*	*82.4*	*71.2*	*78.1*	*71.8*	*60.9*
B	^{1}H	4.93	4.26	3.8	3.54	4.06	1.27
3-α-Rha	^{13}C	*101.4*	*68.4*	*77.5*	*71.4*	*70.2*	*17.9*
C	^{1}H	4.66	3.75	3.57	3.44	3.45	3.74–3.94
t-β-GlcNAc	^{13}C	*104.4*	*56.8*	*74.8*	*71.0*	*77.2*	*62.0*
Before deacetylation		**1**	**2**	**3**	**4**	**5**	**6**
A	^{1}H	5.33	3.60	3.91	3.64	4.01	3.79–3.83
2,4-α-Glc	^{13}C	*96.5*	*82.7*	*71.0*	*78.1*	*71.8*	*61.4*
A'	^{1}H	5.29	3.59	3.9	3.61	4.01	3.79–3.83
2,4-α-Glc	^{13}C	*97.5*	*83.1*	*71.0*	*77.6*	*71.8*	*61.4*
B	^{1}H	4.93	4.26	3.80	3.55	4.08	1.27
3-α-Rha	^{13}C	*101.7*	*68.4*	*77.6*	*71.4*	*70.1*	*17.9*
B'	^{1}H	4.88	4.18	3.75	3.55	4.08	1.27
3-α-Rha	^{13}C	*101.3*	*68.6*	*78.2*	*71.4*	*70.1*	*17.9*
C	^{1}H	4.66	3.75	3.57	3.43	3.48	3.74–3.94
t-β-GlcNAc	^{13}C	*104.4*	*56.8*	*74.7*	*70.8*	*77.2*	*62.0*
C'	^{1}H	4.66	3.76	3.56	3.44	3.69	4.54–4.12
t-β-GlcNAc-6OAc	^{13}C	*104.5*	*56.8*	*74.7*	*71.4*	*74.6*	*65.1*
D	^{1}H	4.92	4.23	3.43	3.49	3.94	1.27
3OMe-α-Rha	^{13}C	*101.7*	*67.3*	*80.8*	*71.4*	*70.3*	*17.6*

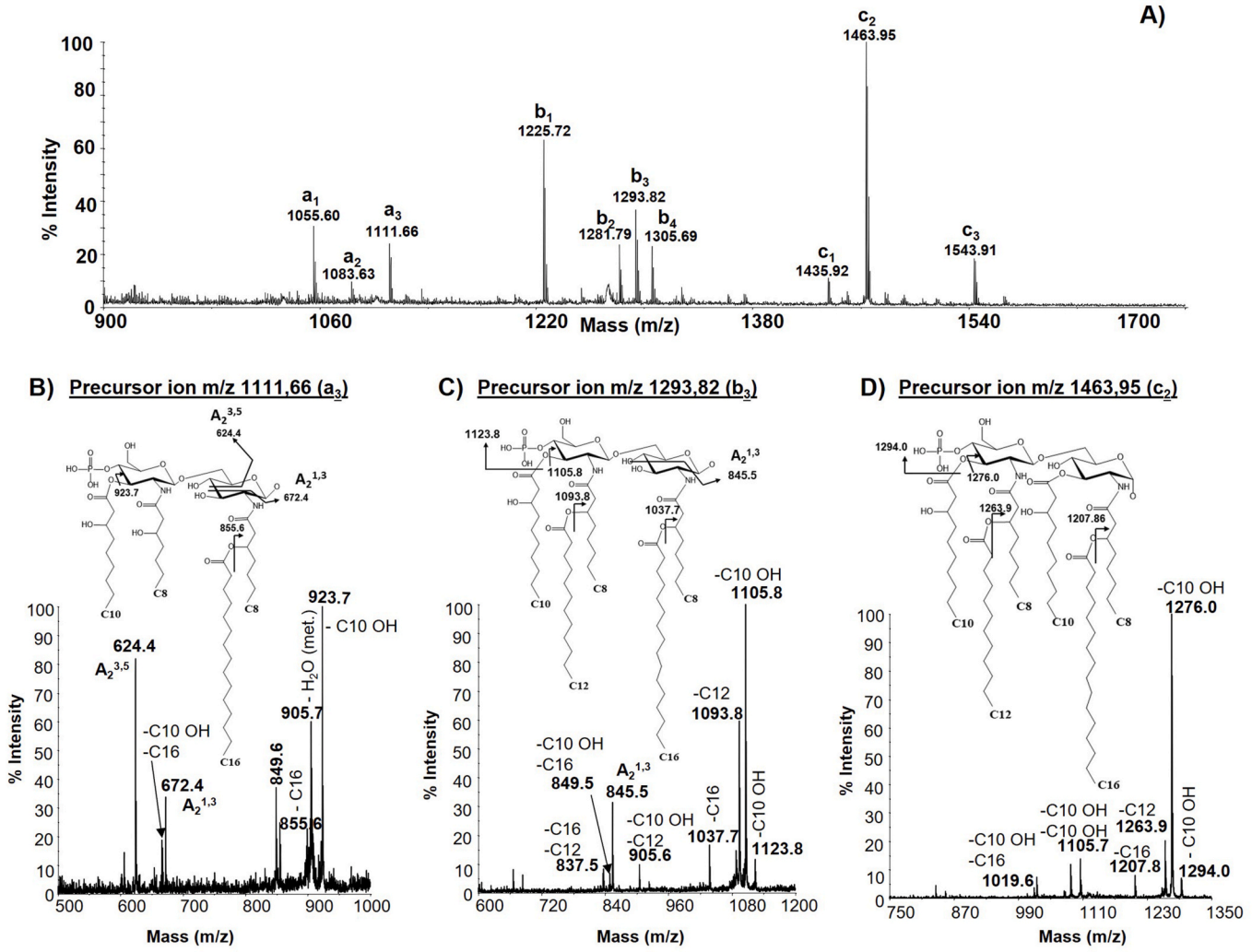

Fig. 5. **A)** Negative-ion MALDI mass spectrum of the lipid A of *D. acidovorans*. **a**, **b** and **c** ion series correspond to tetra, penta and hexa-acylated species, respectively. The composition of each peak is reported in Table S1. **B–D)** MALDI MS/MS spectra and lipid A structures are shown. **B)** tetra-acylated lipid A (**a3** *m/z* 1111.6), **C)** penta-acylated lipid A (**b2** *m/z* 1293.8) and **D)** hexa-acylated lipid A (**c2** *m/z* 1463.9). The assignment of the fragments is reported in the figure.

(3-OH) and a C16:0, in agreement with the compositional analysis. Moreover, the peak at *m/z* 855.6 corresponded to the loss of a C16:0 confirming the composition of the GlcN I. The absence of a peak originating from the loss of C8:0 (3-OH) suggested that this primary fatty acid is amide-linked to both GlcN I and GlcN II. In summary, the MS/MS data indicated that the GlcN II carried an amide linked C8:0 (3-OH) as primary fatty acids and an ester-linked C10:0 (3-OH) without secondary fatty acids, whereas the GlcN I has only one C8:0 (3-OH) amide linked carrying a C16:0 as secondary fatty acid (Fig. S4).

Similarly, the MS/MS analysis of the peak at *m/z* 1293.8 (**b_3**) revealed the structure of the penta-acylated lipid A (Fig. 5C). Indeed, the penta-acylated specie differs from the tetra-acyl specie (**a_3**) only for the composition of the GlcN II as indicated from the fragment $A_2^{1,3}$ (peak at *m/z* 845.5), which disclosed the presence of an additional C12:0. The peaks at *m/z* 1105.8 and *m/z* 1093.8 matched with the loss of C10:0 (3-OH) and C12:0, respectively, thus confirming the composition of the GlcN II. In addition, the absence of peaks originated from the loss of hydroxylated fatty acids bearing a C12:0 as secondary fatty acid, suggested that this secondary fatty acid is located at the amide linked C8:0 (3-OH) of the GlcN II. As for GlcN I, it had the same substitution pattern the tetra-acylated specie (**a_3**), and also in this case, it was observed the loss of C16:0 (peak at *m/z* 1037.7). The MS/MS analysis on the precursor ion at *m/z* 1463.9 (**c_2**) (Fig. 5D) allowed to elucidate the structure of the hexa-acylated lipid A. The peak at *m/z* 1105.7 indicated the loss of two unsubstituted C10:0 (3-OH), thus revealing that both glucosamines had one ester-linked C10:0 (3-OH) as primary fatty acid. Furthermore, the loss of C10:0 (3-OH), C12:0 and C 16:0, clearly defined the structure of hexa-acylated lipid A. In detail, the GlcN II shared the same composition of the corresponding residue of the penta-acylated species **b_3**, while GlcN I had a further C10:0 (3-OH) as primary ester linked fatty acid (Fig. S4).

In conclusion, the analysis of Delftia lipid A revealed that the backbone of glucosamine of all species has in common two C8:0 (3-OH) in amide linkage and one or two C10:0 (3-OH) in ester linkage as primary fatty acid. Furthermore, depending on the species, GlcN I could have a C12:0, a C14:0 or C16:0 linked to the 3-hydroxyl function of the C8:0, while the GlcN II could carry or not C12:0 as secondary fatty acid linked to the amide-linked C8:0 (3-OH) (Fig. S4).

4. Conclusions

This study presents the first known characterization of O-antigen and lipid A in the *Delftia* genus. The O-antigen structure of the lipopolysaccharide (LPS) from *Delftia acidovorans* represents a novel glycan structure, as there are no matches in the Carbohydrate Structure Database (CSDB, search at 25-10-2024). This structure consists of glucose and rhamnose in the linear backbone [3)-α-L-Rha-(1 → 4)-α-D-glucose-(1→], where the glucose is further glycosylated at position O-2 with a α-D-N-

acetyl-glucosamine. Additionally, the N-acetyl-glucosamine can be further acetylated at position O-6. Interestingly, the acetylation at O-6 of the N-acetyl-glucosamine was never found in Betaprotobacteria. At the same time, it is a common sugar modification found in the O-antigen of the Gammaproteobacteria, such as Proteus [12], Shigella [13], and Pseudomonas putida [14].

Regarding the lipid A portion of *D. acidovorans*, it is represented by tetra-, penta- and hexa-acylated species, where the hexa-acylated is the predominant one, similarly to those of other *Delftia* [16]. All the species have a backbone of bis-phosphorylated disaccharide of D-glucosamine carrying as primary fatty acid two C8:0 (3-OH) in amide linkage and one or two C10: 0 (3-OH) in ester linkage, while the secondary fatty acids (C12:0, C 14:0, C 16:0) vary according to the species considered. Results that are in accordance with the analysis of the cell fatty acids of *D. acidovorans* strain ESM-1 [15]. The hexa-acylated specie exhibits a symmetric acylation pattern, known as 3 + 3 symmetry, as the lipid A of *Neissera meningitidis* [16]. It is well established that the length and the distribution of the fatty acids dramatically influence the immunostimulatory effect of the lipid A molecule. Therefore, this research paves the way for future studies aimed at understanding the role that these molecules play within the crypt-specific core microbiota of healthy mice, investigating how and if this peculiar structure impacts on its role.

CRediT authorship contribution statement

Anna Notaro: Writing – original draft, Visualization, Methodology, Investigation, Formal analysis. **Luisa Sturiale:** Visualization, Methodology, Investigation, Formal analysis. **Angelo Palmigiano:** Visualization, Methodology, Investigation, Formal analysis. **Domenico Garozzo:** Writing – review & editing. **Immacolata Speciale:** Writing – review & editing, Writing – original draft, Supervision, Conceptualization.

Declaration of competing interest

The authors declare that they have no known competing financial interests or personal relationships that could have appeared to influence the work reported in this paper.

Acknowledgments

The authors express their sincere gratitude to Thierry Pédron from the Institut Pasteur in Paris, France, for providing the *D. acidovorans* bacterium, which was isolated from the proximal tissues of healthy mice.

Appendix A. Supplementary data

Supplementary data to this article can be found online at https://doi.org/10.1016/j.carres.2025.109586.

Data availability

Data will be made available on request.

References

[1] A. Wen, M. Fegan, C. Hayward, S. Chakraborty, L.I. Sly, Phylogenetic relationships among members of the Comamonadaceae, and description of Delftia acidovorans (den Dooren de Jong 1926 and Tamaoka et al. 1987) gen. nov., comb. nov, Int. J. Syst. Bacteriol. 49 Pt 2 (1999) 567–576, https://doi.org/10.1099/00207713-49-2-567.

[2] N. Agarwal, A. Jindal, A. Bhargava, Delftia acidovorans : rarely a pathogen: a case report, Pediatr. Infect. Dis. J. 42 (2023) e130–e131, https://doi.org/10.1097/INF.0000000000003818.

[3] O.I. Sazonova, A.A. Ivanova, Y.A. Delegan, R.A. Streletskii, D.D. Vershinina, S. L. Sokolov, A.A. Vetrova, Characterization and genomic analysis of the naphthalene-degrading Delftia tsuruhatensis ULwDis3 isolated from seawater, Microorganisms 11 (2023), https://doi.org/10.3390/microorganisms11041092.

[4] S.M.M. Højgaard, O. Rezahosseini, J.D. Knudsen, N.J.U. Fuglebjerg, M. Skov, S. D. Nielsen, Z.B. Harboe, Characteristics and outcomes of patients with Delftia acidovorans infections: a retrospective cohort study, Microbiol. Spectr. 10 (2022), https://doi.org/10.1128/spectrum.00326-22.

[5] R. Funari, R. Ripa, B. Söderström, U. Skoglund, A.Q. Shen, Detecting gold biomineralization by Delftia acidovorans biofilms on a quartz crystal microbalance, ACS Sens. 4 (2019) 3023–3033, https://doi.org/10.1021/acssensors.9b01580.

[6] A. Notaro, A. Vanacore, A. Molinaro, I. Speciale, C. De Castro, Structure and conformation study of the O-Antigen from the lipopolysaccharide of Cupriavidus metallidurans CH34, Polysaccharides 3 (2022) 188–199, https://doi.org/10.3390/polysaccharides3010009.

[7] M.C. Ubalde, V. Braña, F. Sueiro, M.A. Morel, C. Martínez-Rosales, C. Marquez, S. Castro-Sowinski, The versatility of Delftia sp. isolates as tools for bioremediation and biofertilization technologies, Curr. Microbiol. 64 (2012) 597–603, https://doi.org/10.1007/s00284-012-0108-5.

[8] M.G. Romanelli, S. Povolo, L. Favaro, F. Fontana, M. Basaglia, S. Casella, Engineering Delftia acidovorans DSM39 to produce polyhydroxyalkanoates from slaughterhouse waste, Int. J. Biol. Macromol. 71 (2014) 21–27, https://doi.org/10.1016/j.ijbiomac.2014.03.049.

[9] H. Hagiya, T. Murase, J. Sugiyama, Y. Kuroe, H. Nojima, H. Naito, S. Hagioka, N. Morimoto, Delftia acidovorans bacteremia caused by bacterial translocation after organophosphorus poisoning in an immunocompetent adult patient, J. Infect. Chemother. 19 (2013) 338–341, https://doi.org/10.1007/s10156-012-0472-x.

[10] K. Chotikanatis, M. Bäcker, G. Rosas-Garcia, R. Hammerschlag Margaret, Recurrent intravascular-catheter-related bacteremia caused by Delftia acidovorans in a hemodialysis patient, J. Clin. Microbiol. 49 (2020) 3418–3421, https://doi.org/10.1128/jcm.00625-11.

[11] K.J. Lang, T. Chinzowu, K.J. Cann, Delftia acidovorans as an unusual causative organism in line-related sepsis, Indian J. Microbiol. 52 (2012) 102–103, https://doi.org/10.1007/s12088-011-0221-3.

[12] H. Bilgin, A. Sarmis, E. Tigen, G. Soyletir, L. Mulazimoglu, Delftia acidovorans: a rare pathogen in immunocompetent and immunocompromised patients, Can. J. Infect. Dis. Med. Microbiol. 26 (2015) 277–279, https://doi.org/10.1155/2015/973284.

[13] C. Ta, G. Wong, W. Cole, G. Medvedev, Scrub sink contamination and transmission to operating room personnel, New Microbes New Infect 37 (2020) 100754, https://doi.org/10.1016/j.nmni.2020.100754.

[14] M.H. Yassin, B. Abramovitz, R. Hariri, L. McKibben, A.J. Pinevich, Delftia acidovorans pseudo outbreak in portable reverse osmosis machines: interventions to ensure safe and cost-effective hemodialysis, Am. J. Infect. Control 48 (2020) 304–308, https://doi.org/10.1016/j.ajic.2019.11.027.

[15] T. Pédron, C. Mulet, C. Dauga, L. Frangeul, C. Chervaux, G. Grompone, J. Sansonetti Philippe, A crypt-specific core microbiota resides in the mouse Colon, mBio 3 (2012), https://doi.org/10.1128/mbio.00116-00112.

[16] T. Naito, C. Mulet, C. De Castro, A. Molinaro, A. Saffarian, G. Nigro, M. Bérard, M. Clerc, A.B. Pedersen, P.J. Sansonetti, T. Pédron, Lipopolysaccharide from crypt-specific core microbiota modulates the colonic epithelial proliferation-to-differentiation balance, mBio 8 (2017), https://doi.org/10.1128/mBio.01680-17.

[17] F. Di Lorenzo, K.A. Duda, R. Lanzetta, A. Silipo, C. De Castro, A. Molinaro, A journey from structure to function of bacterial lipopolysaccharides, Chem Rev 122 (2022) 15767–15821, https://doi.org/10.1021/acs.chemrev.0c01321.

[18] C. De Castro, M. Parrilli, O. Holst, A. Molinaro, Microbe-associated molecular patterns in innate immunity: extraction and chemical analysis of gram-negative bacterial lipopolysaccharides, Methods Enzymol. 480 (2010) 89–115, https://doi.org/10.1016/S0076-6879(10)80005-9.

[19] O. Westphal, K. Jann, Bacterial lipopolysaccharides : extraction with phenol-water and further applications of the procedure, Methods in Carbohydrate Chem 5 (1965) 83–91.

[20] R. Kittelberger, Sensitive silver-staining detection of bacterial lipopolysaccharides in polyacrylamide gels, J. Biochem. Biophys. Methods 26 (1993) 81–86, https://doi.org/10.1016/0165-022x(93)90024-i.

[21] P. Garcia-Vello, I. Speciale, F. Di Lorenzo, A. Molinaro, C. De Castro, Dissecting lipopolysaccharide composition and structure by GC-MS and MALDI spectrometry, Methods Mol. Biol. 2548 (2022) 181–209, https://doi.org/10.1007/978-1-0716-2581-1_12.

[22] K. Leontein, B. Lindberg, J. Lonngren, Assignment of absolute configuration of sugars by g.l.c. of their acetylated glycosides formed from chiral alcohols, Carbohydr. Res. 62 (1978) 359–362, https://doi.org/10.1016/S0008-6215(00)80882-4.

[23] L. Sturiale, A. Palmigiano, A. Silipo, Y.A. Knirel, A.P. Anisimov, R. Lanzetta, M. Parrilli, A. Molinaro, D. Garozzo, Reflectron MALDI TOF and MALDI TOF/TOF mass spectrometry reveal novel structural details of native lipooligosaccharides, J. Mass Spectrom. 46 (2011) 1135–1142, https://doi.org/10.1002/jms.2000.

[24] J. Lönngren, S. Svensson, Mass spectrometry in structural analysis of natural carbohydrates, Adv. Carbohydr. Chem. Biochem. 29 (1974) 41–106, https://doi.org/10.1016/s0065-2318(08)60248-6.

[25] I. Speciale, A. Notaro, P. Garcia-Vello, F. Di Lorenzo, S. Armiento, A. Molinaro, R. Marchetti, A. Silipo, C. De Castro, Liquid-state NMR spectroscopy for complex carbohydrate structural analysis: a hitchhiker's guide, Carbohydr. Polym. 277 (2022) 118885, https://doi.org/10.1016/j.carbpol.2021.118885.

[26] V. Laplanche, S. Armiento, I. Speciale, T. Šuligoj, E.H. Crost, D. Lamprinaki, L. Vaux, K. Gotts, C. De Castro, N. Juge, The human gut symbiont Ruminococcus gnavus displays strain-specific exopolysaccharides modulating the host immune response, Carbohydr. Polym. 347 (2025), https://doi.org/10.1016/j.carbpol.2024.122754.